Reversal of exchange bias in nanocrystalline antiferromagnetic–ferromagnetic bilayers

2002 J. Phys.: Condens. Matter 14 10063

(http://iopscience.iop.org/0953-8984/14/43/305)

INSTITUTE OF PHYSICS PUBLISHING JOURNAL OF PHYSICS: CONDENSED MATTER

J. Phys.: Condens. Matter **14** (2002) 10063–10074 PII: S0953-8984(02)39059-3

Reversal of exchange bias in nanocrystalline antiferromagnetic–ferromagnetic bilayers

C Prados[1], **E Pina**[1,3], **A Hernando**[1] **and A Montone**[2]

[1] Instituto de Magnetismo Aplicado, RENFE-UCM-CSIC, PO Box 155, Las Rozas 28230 Madrid, Spain
[2] ENEA, Materials and Technology Unit, CR Casaccia, CP 2400, 00100 Rome, Italy

E-mail: epina@renfe.es

Received 1 July 2002, in final form 19 September 2002
Published 18 October 2002
Online at stacks.iop.org/JPhysCM/14/10063

Abstract

The sign of the exchange bias in field cooled nanocrystalline antiferromagnetic–ferromagnetic bilayers (Co–O and Ni–O/permalloy) is reversed at temperatures approaching the antiferromagnetic (AFM) blocking temperature. A similar phenomenon is observed after magnetic training processes at similar temperatures. These effects can be explained assuming that the boundaries of nanocrystalline grains in AFM layers exhibit lower transition temperatures than grain cores.

1. Introduction

Exchange anisotropy refers to the interface interaction between ferromagnetic (FM) and antiferromagnetic (AFM) materials. When a AFM/FM thin film bilayer is cooled through the Néel (T_N) temperature of the AFM (with the Curie temperature T_C of the FM larger than T_N) in a saturating magnetic field, a unidirectional anisotropy is induced in the FM. This anisotropy is commonly manifested as, among other things, a hysteresis loop shifted towards fields *opposite* to that applied during the cooling process, an enhancement of coercivity and a $\sin\theta$ component in the torque curve. The strength of the exchange anisotropy is usually quantified by the shift of the hysteresis loop, which is called the exchange field, H_E. Although this phenomenon was first reported a long time ago in passivated Co particles [1], a great number of experimental and theoretical works were afterwards developed, many of them reported in reviews [2] and [3], due to the intriguing physics underlying this interface exchange coupling and its practical applications. In fact, exchange anisotropy is systematically used for controlling the direction of magnetization in magneto-electronic devices, such as spin valves in magnetic storage read heads [4]. In addition to the above-described features, exchange-biased bilayers also can exhibit several less usual properties, such as positive exchange bias [5, 6], magnetic training effects [7], asymmetric magnetization reversal processes [8] and memory effects [9].

[3] Author to whom any correspondence should be addressed.

An intuitive picture of the exchange anisotropy mechanism has already been proposed in the early works of Meiklejohn and Bean [1], based on an uncompensated AFM interface and the interfacial exchange interaction between the AFM–FM spins. However, there is little quantitative understanding of the phenomenon and the development of an ultimate theoretical framework accounting for the different aspects of the unidirectional anisotropy remains elusive. Different theories have been proposed since the earlier works, in which collinear magnetic structures on both FM and AFM sides of the interface were assumed. Most of these theories, reported in reviews [10, 11], propose more complex interfaces that better approach the actual ones. We will focus on theoretical models adequate for polycrystalline thin film systems, similar to those studied here. Two main trends can be distinguished in such theoretical models explaining the exchange anisotropy, mainly concerning the magnitude of H_E. Firstly, some works propose the existence of a domain structure parallel to the interface, either in the AFM or the FM material [12]. This approach has been used to explain different properties related to the exchange anisotropy, such as irreversible [13] and memory [9] effects. Another general approach assumes the formation of AFM domains perpendicular to the interface plane. Malozemoff [14] considers a random exchange interaction at the interface due to the surface roughness or chemical inhomogeneity at atomic scale. The interfacial random-field energy is minimized when the AFM breaks up into a perpendicular domain structure. Within this trend we can also include works related to exchange anisotropy in polycrystalline systems. Takano *et al* [15] suggest that uncompensated spins on the surface of AFM films are responsible for unidirectional anisotropy. The origin of this uncompensated moment lies in the finite grain size of the AFM film. In this way, the AFM grains play a similar role to the perpendicular AFM domains in Malozemoff's approach.

In this paper we report measurements on thermal evolution of coercivity, H_c, and the exchange field, H_E, in nanocrystalline Co–O/permalloy (Py) and Ni–O/Py bilayers after different cooling and training processes. Since the uncompensated moment related to the finite size of the AFM grains seems to be the source of the exchange anisotropy in this kind of structure, enhanced interfacial effects are expected when grain size is decreased [16]. In particular, we report new and striking phenomena consisting in a reversal of sign in exchange anisotropy when temperature is increased in the region just below the AFM transition. This behaviour is related to the existence of two different magnetic transition temperatures in the AFM layers, one of them corresponding to grain boundaries and the other to grain cores. Finally, a simple phenomenological model is developed to account for the relation between the described experimental results concerning the reversal of exchange bias and the nanocrystalline nature of the samples.

2. Sample preparation and structural characterization

Co–O (20 nm)/Py (20 nm) and Ni–O (40 nm)/Py (20 nm) bilayer samples were grown by rf magnetron sputtering onto 1 mm thick glass substrates at nominal room temperature. The background pressure was lower than 5×10^{-7} mbar. Oxide layers were reactively sputtered from pure Co and Ni targets. The sputtering gas during reactive deposition of layers was oxygen up to 2×10^{-3} mbar and Ar up to 5×10^{-3} mbar. Py layers were deposited from composite targets using Ar at 5×10^{-3} mbar. A final Cu layer was added as an oxidation barrier. Deposition rate calibration of the individual layers was carried out by low-angle x-ray diffraction, being 0.1 nm s^{-1} (Py), 0.03 nm s^{-1} (Co–O) and 0.07 nm s^{-1} (Ni–O), respectively. These conditions were revealed as the most appropriate for growing thin films in our sample preparation system with the required nanocrystalline structure.

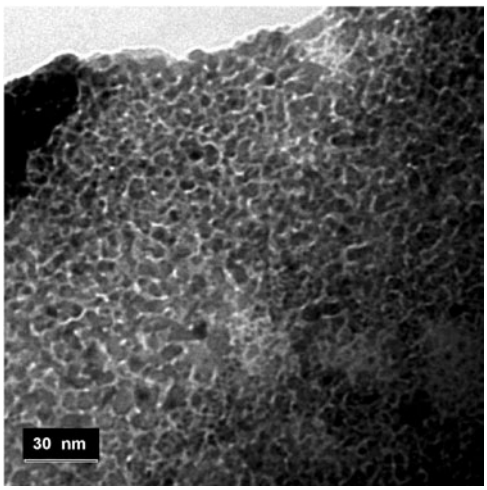

Figure 1. Planar-view TEM image of a Co–O (20 nm) layer deposited onto 1 mm glass substrate. The image is slightly out of focus to enhance phase contrast at the grain boundaries.

Separate control samples of both Ni and Co oxides were also prepared under identical oxygen reactive sputtering conditions in order to carry out a deeper analysis of the crystalline structure of the AFM layers. Hence, a 20 nm thickness Co–O layer and a 40 nm thickness Ni–O layer were grown onto 1 mm thick glass substrates.

Structural characterization of samples was performed by transmission electron microscopy (TEM) with a JEOL 4000FX microscope operating at 300 kV equipped with ultra-thin window x-ray detector and imaging electron spectrometer. Samples, in plan and cross-section geometry, were prepared with the usual method of grinding, dimpling and ion beam milling at glazing angle. Planar-view images were taken from Co–O and Ni–O single-layer specimens revealing a quasi-spherical grain shape with a log-normal distribution of grain diameters centred at 3.9 and 5.3 nm, respectively. Figure 1 shows a bright-field planar-view image of the Co–O sample. Besides the clear nanocrystalline structure, the image, which is slightly out of focus to enhance the phase contrast, shows a remarkable phase contrast at the grain boundaries. This fact indicates compositional or structural differences between boundaries and cores which will be reflected in the magnetic properties. The estimated thickness of boundaries in both cases is around 0.5 nm. Cross-sectional images of bilayers were taken in order to observe the interaction interface between AFM and FM layers as well as the lateral dimensions of grains. Figure 2 shows a bright-field cross-sectional image of a Co–O/Py sample from which a statistical value of 14.2 nm for the grain size of Py grains has been determined. A well defined interface with a roughness less than 3 nm is also observed. X-ray microanalysis and microdiffraction confirm the presence of a sharp interface within the relative spatial resolutions.

3. Magnetization measurements

3.1. Thermal evolution of hysteresis

Magnetization measurements were carried out by using a Quantum Design SQUID magnetometer. Magnetic field was always applied parallel to the film plane and magnetic moment was measured along the field direction. Co–O/Py bilayers were cooled from 300 to 50 K in the presence of a saturating magnetic field of +1 kOe. Figure 3 shows three consecutive

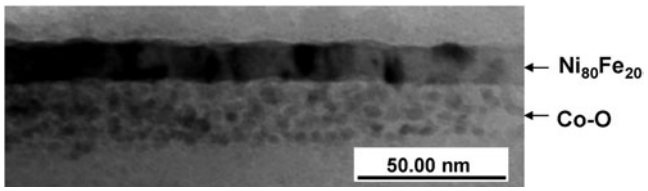

Figure 2. Cross-sectional view TEM image of a Co–O (20 nm)/Py (20 nm) bilayer deposited onto 1 mm glass substrate.

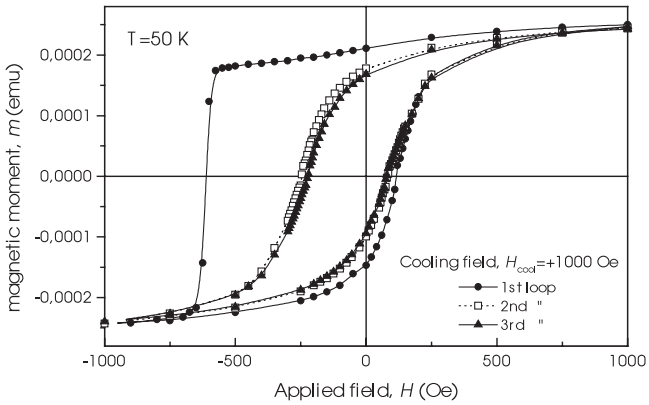

Figure 3. Three consecutive hysteresis loops for a Co–O (20 nm)/Py (20 nm) bilayer measured at 50 K after cooling the sample in a field $H_{cool} = +1000$ Oe. A huge training effect of shift and coercivity is observed after the first cycle.

hysteresis loops which were measured at 50 K immediately after the field cooling process. The shift of the loops towards negative fields and the enhanced coercivity indicate the presence of exchange anisotropy induced by the field cooling process. The huge decrease of coercivity and exchange field after the first consecutive loops indicates the existence of a sizeable number of biased spins belonging to the AFM layer in metastable spin configurations. After each magnetization cycle the AFM spins evolve to energetically favourable configurations. In this way, the training process erases partially the initial spin distribution and, hence, it provokes a decrease of exchange anisotropy effects. Since nanocrystalline structure implies a large ratio of spins located at grain boundaries, where their disordered structure brings out fluctuations in magnetic anisotropy and exchange strength, the training effect is strongly reinforced by the reduced grain size of the AFM layer.

After the magnetic training at 50 K, hysteresis loops were measured at different temperatures between 50 and 300 K. Figures 4(a) and (b) show the evolution of H_c and H_E with temperature for the sample Co–O (20 nm)/Py (20 nm). The first result is that the temperature above which exchange anisotropy effects disappear is around 200 K, well below the T_N of bulk CoO ($T_N = 293$ K). This transition temperature, called the blocking temperature, T_B, is in the lower range of previously reported values for polycrystalline CoO [2] and reflects the influence of the reduced grain size ($T_B = 175$ K is reported in [17] for a 20 Å CoO/164 Å Co bilayer). Three regions can be distinguished in the thermal evolution of H_E:

(i) at low temperatures the hysteresis loops are shifted towards negative fields and the absolute value of H_E decreases with the increase of temperature (this is the most usual behaviour for a positive cooling field),

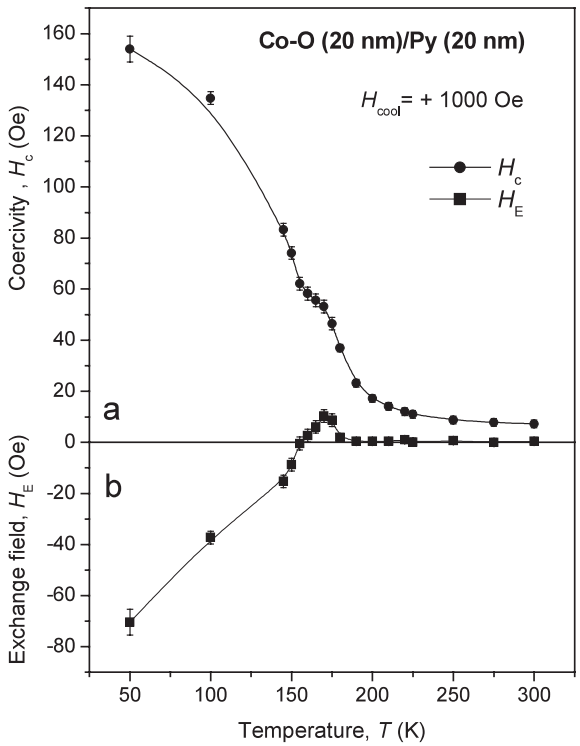

Figure 4. Thermal evolution of coercivity (a) and loop shift (b) for a Co–O (20 nm)/Py (20 nm) bilayer measured after cooling the sample in a field $H_{cool} = +1000$ Oe from 300 to 50 K and three training cycles at 50 K. Positive exchange bias is observed between 150 and 180 K.

(ii) as the temperature approaches the AFM blocking temperature, a particular effect occurs, the sign of H_E is reversed (above ∼150 K), i.e., the loops are shifted towards *positive* fields, and

(iii) after reaching a maximum positive value around 170 K, the unidirectional anisotropy disappears above 200 K.

Figure 4(a) shows the evolution of coercivity along different measurement temperatures. It decreases monotonically with the increasing temperature and exhibits an enhanced value below the blocking temperature of the AFM layer. A characteristic feature is observed (which is discussed below) at temperatures where reversal of exchange field appears. Similar behaviour is observed in nanocrystalline Ni–O/Py bilayers. In that case the samples have been field cooled from 400 to 50 K under +1 kOe and data have been measured after training the sample at 50 K. The measured Ni–O blocking temperature is around 375 K and positive shifted loops are observed above 300 K (figure 5).

The experimental validity of the results presented in this work has been tested in two ways. Firstly, the above-described hysteretic measurements have been repeated up to four times in different runs. In this way, each experimental point in figures 4 and 5 is the result of a statistical average over a number of different measurements. Error bars correspond to the standard deviation and always are much smaller than the magnetic features related to the reversal effect. In some cases, error bars are smaller than the symbols. On the other hand, the experiments in both kinds of bilayer have been repeated cooling the samples under the

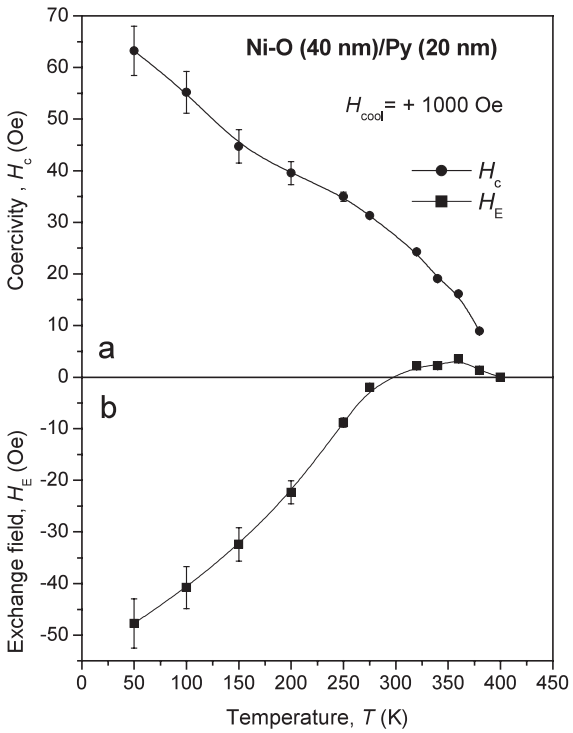

Figure 5. Thermal evolution of coercivity (a) and loop shift (b) for a Ni–O (40 nm)/Py (20 nm) bilayer measured after cooling the sample in a field $H_{cool} = +1000$ Oe from 400 to 50 K and three training cycles at 50 K. Positive exchange bias is observed between 300 and 400 K.

highest available field (+55 kOe). Results are identical, but affected by larger experimental error due to remanent currents in the superconducting coil. This new set of measurements was performed in order to discard minor loop effects at low temperatures.

3.2. Magnetic training at fixed temperatures

Reversal of exchange anisotropy sign has been also observed after training the samples at a fixed temperature close to the AFM transition. The measurement procedure was as follows: the bilayer was cooled under an applied field of +1 kOe from 300 K (400 K in the case of bilayers with Ni–O as AFM layer) to the measurement temperature, T_m (special precautions were taken in order to avoid undercooling), and then consecutive loops were measured with applied fields in the +1 to −1 kOe range. The same cooling procedure was performed for each measurement temperature. Figure 6(b) shows the evolution of H_E for three consecutive loops after cooling the sample according to the above-described procedure to temperatures between 120 and 200 K. In the low-temperature range, H_E is always negative and its absolute value decreases with consecutive cycles. However, at temperatures between 150 and 160 K, whereas the first loop shows negative exchange anisotropy, successive cycles are shifted towards positive fields. Immediately before the AFM transition, even the first loop exhibits a positive shift, of which the absolute value decreases after the second one. Figure 6(a) shows the evolution of coercivity for different measurement temperatures.

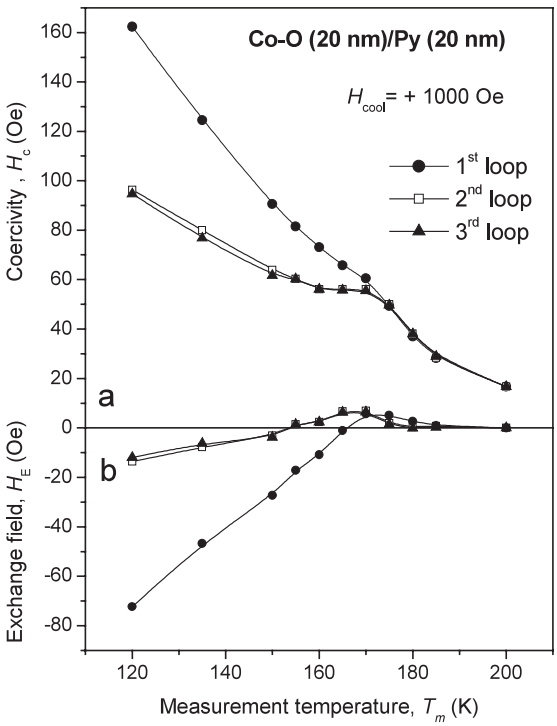

Figure 6. Evolution of coercivity (a) and loop shift (b) of three consecutive loops measured after cooling the sample in a field $H_{cool} = +1000$ Oe from 300 K with measurement temperature T_m. The sample is a Co–O (20 nm)/Py (20 nm) bilayer. Training induced reversal of the exchange anisotropy is observed between 155 and 170 K.

4. Analysis and discussion

Positive unidirectional exchange anisotropy has been reported in thin film bilayers cooled under large magnetic fields [18]. Those results were attributed to the combination of an AFM exchange through the AFM–FM interface and an FM alignment of the AFM surface spins along the large cooling field. In the present work, we have observed a change of sign of exchange bias in bilayers cooled under moderate (but saturating) magnetic fields. Following a similar approach to that developed in [15], we consider the antiferromagnet as a set of crystallites, which exhibit individually a rather compensated spin structure at the interface with the ferromagnet. The finite size of the grains implies uncompensation of magnetic moment at the AFM/FM interface. This uncompensated moment is mainly located at the grain boundaries of the AFM layer. Due to the structural disorder associated with the grain boundary, anisotropy, exchange coupling and magnetic transition temperatures will be expected to be different to those within grain cores. These particularities become sizeable in nanostructured materials, with a large ratio of spins located at grain boundaries [19, 20]. In our case, the structural characterization of oxide layers showed the existence of a grain boundary region clearly differentiated from grain cores. A reduced transition temperature is expected in the AFM grain boundaries as a consequence of the finite-size scaling effect [21]. For the sake of simplicity, we are going to consider the interfacial AFM–FM interaction as FM direct exchange coupling and therefore, during the cooling process, the uncompensated moment in the AFM

layer would align parallel to the magnetization in the FM (any other mechanism of coupling would not modify the explanation developed below). The rest of the AFM spins will arrange accordingly, and this particular spin configuration will remain frozen giving rise to negative shifted hysteresis loops. The mechanism that we propose to account for the observed reversal of exchange anisotropy assumes different blocking temperatures for boundary and core regions: we define $T_{B,c}$ as the blocking temperature of the core regions and we can consider a gradient of blocking temperatures at the boundary region with $T_{B,b}$ as the lower one ($T_{B,b} < T_{B,c}$). Below $T_{B,b}$ the uncompensated moment is principally located at grain boundaries and it lies within the direction of the cooling field. When $T_{B,b} < T < T_{B,c}$ the grain boundary region becomes paramagnetic as the temperature increases. The uncompensated moment will decrease in absolute value and eventually will reverse its sign due to the AFM nature of the magnetic order of the oxide layer. In this framework, the thermal evolution of H_E can be explained as follows.

(i) After cooling the system in a positive field, the hysteresis loops are shifted towards negative fields at low temperature due to the positive AFM uncompensated moment. Strong training effects are observed as shown in figure 3 due to the disordered nature of the grain boundary region.
(ii) As temperature increases and approaches the overall magnetic transition of the AFM layer, grain boundaries of the oxide (where the uncompensated magnetic moment is located) becomes paramagnetic. The AFM nature of the oxide layer makes, as the grain boundary region loses its magnetic order, the grain cores exhibit *negative* uncompensated magnetic moment. Therefore, *positive* shift is induced in the hysteresis loop of the FM layer.
(iii) Finally, above the AFM transition temperature, exchange anisotropy disappears.

In a similar way it is possible to account for results such as those shown in figure 6. After cooling the sample under a positive field to a given temperature close to the transition, the first hysteresis loop will exhibit negative shift. Subsequent training of the sample will produce strong magnetic relaxation of grain boundaries and the resulting uncompensated moment will give positive shift of the FM loops.

We have developed a simple qualitative model in order to show how, as the boundaries of a set of AFM grains lose magnetic order with increasing temperature, the sign of the uncompensated moment is reversed. We have calculated the thermal evolution of the uncompensated moment in a certain distribution of bidimensional AFM grains. Firstly, we consider the contact interface to be a plane with an AFM arrangement of spins, as shown in the idealized top view in figure 7. In order to make a realistic approximation we consider such an interface to be formed by circular grains with ratio R (figure 7), reflecting the AFM grains in the TEM images (figure 1). Within each grain the spins are arranged in a squared lattice whose parameter will be related to the actual parameter of studied oxides. Let us define the net moment per unit area of one of these AFM grains as

$$m_R = \frac{\sum_{i^2+j^2 \leqslant R^2} (-1)^{i+j}}{\pi R^2}. \tag{1}$$

The AF configuration providing a positive uncompensated moment has been selected between the two possible spin arrangements for each grain, in order to simulate the field cooling process carried out in the magnetic measurements. For that, the following initial condition is taken:

$$\sum_{i^2+j^2 \leqslant R^2} (-1)^{i+j} > 0. \tag{2}$$

In order to simulate the increase of temperature, we eliminate the magnetic moment of those spins placed in the grain boundary. Hence, we define a magnetic ratio R_{mag} in such a way

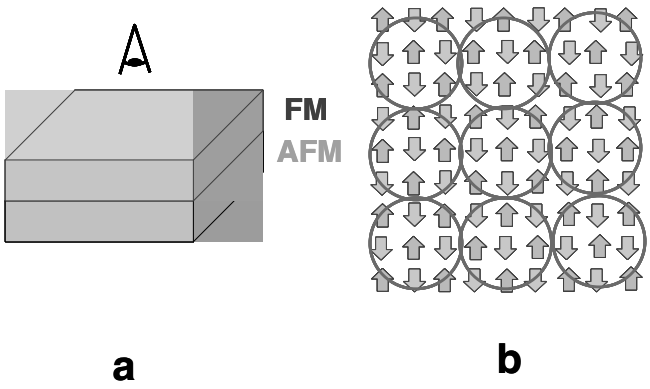

Figure 7. Schematic top view of the contact AFM–FM interface (a) and distribution of AFM grains with circular symmetry (b) from the perspective of the right-hand figure.

that the magnetic order only exists within the grain (see figure 8). We define a new parameter that is the relative thickness of the non-magnetic grain shell:

$$t_f = R - R_{mag} \tag{3}$$

where R and R_{mag} are referred to the lattice parameter (t_f is a non-dimensional parameter). The decrease of the magnetic diameter R_{mag}, i.e. the increase of t_f, accounts for the progressive magnetic transition of the grain boundary region induced by increasing temperature. According to the results of TEM studies, we consider a log-normal grain size distribution centred on an average ratio R_0. The total uncompensated magnetic moment of such a distribution will be given by the following expression:

$$M_{R_0} = k \sum_{R} \exp\left(-\frac{\left[\ln \frac{R}{R_0}\right]^2}{2\sigma^2}\right) \sum_{i^2+j^2 \leqslant R_{mag}^2} (-1)^{i+j}. \tag{4}$$

Figure 9 shows the evolution of the total uncompensated magnetic moment as a function of the thickness of the paramagnetic shell for sets of AFM grains with different diameter distributions, calculated according to equation (4). Grain diameter distributions are centred between 2.0 and 3.5 nm and the distribution width is in all cases 2.0 nm (parameters have been obtained from the analysis of bright-and dark-field TEM images corresponding to cobalt oxide). The initial uncompensated moment is positive and its value per unit area decreases with the increase of the average grain diameter. As the grain boundary becomes paramagnetic, the uncompensated moment decreases and, due to the AFM coupling within the grains, eventually changes to negative when the thickness of the paramagnetic shell is of the order of one lattice parameter ($a = 0.427$ nm for Co–O [22]). This result is in good agreement with those from the structural analysis in which a typical value of 0.5 nm was obtained for the grain boundary thickness. This fact indicates that the total transition of the grain boundary to the paramagnetic state is responsible for the change of sign in the uncompensated AF moment.

Most of the magnetic quantitative features related to exchange anisotropy have not been satisfactorily explained yet, but some qualitative aspects, such as the relation between the magnitudes of shift [2] and coercivity enhancement [23], have been directly connected to the strength of the interfacial coupling through the AFM/FM interface. Therefore, both magnitudes, H_E and H_c, will be a function of the uncompensated interfacial moment, and their thermal evolution will reflect the thermal dependence of this uncompensated magnetic

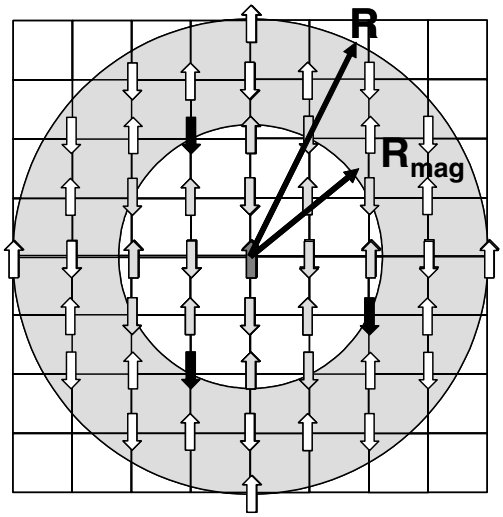

Figure 8. Scheme of one AFM grain with a total ratio R and a magnetic ratio R_{mag}. Notice that, eliminating the spins on the boundary (white arrows), the uncompensated moment (black arrows) is placed now on the border of the inner ratio (R_{mag}).

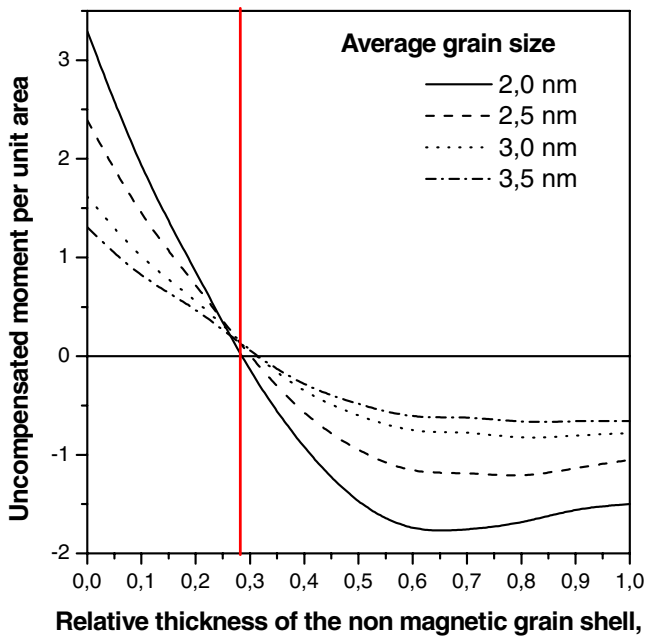

Figure 9. Uncompensated moment per unit area of a set of bidimensional AFM grains with different average grain size calculated as a function of the relative thickness of the non-magnetic shell t_f. The initial spin configuration ($t_f = 0$) has been selected to provide a positive uncompensated moment in each grain, in order to simulate a field cooling process. Curves sketch the reversal of the uncompensated moment induced by the magnetic transition of the grain boundary.

(This figure is in colour only in the electronic version)

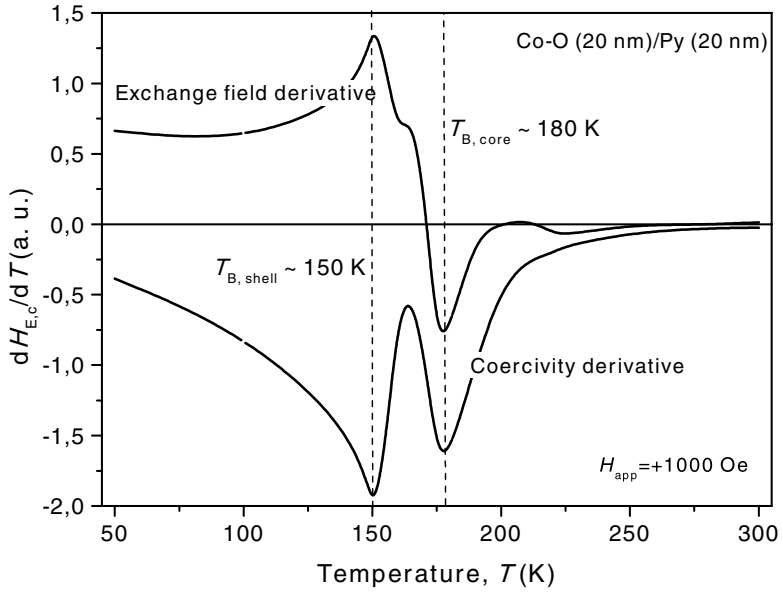

Figure 10. Thermal evolution of temperature derivative of exchange field and coercivity performed from experimental data shown in figure 2. Two transition temperatures appear: the first one (∼150 K) is related to the magnetic transition of grain boundaries and the higher one (∼180 K) to the transition of grain cores of the AFM layer.

moment. Figure 10 shows the temperature derivative of the experimental data corresponding to H_E and H_c for CoO/Py bilayers (shown in figure 4) where two transition temperatures are clearly distinguished. The lower one, $T_{B,b} \sim 150$ K, is identified as the blocking temperature of the uncompensated moment of the AFM grain boundaries, and it corresponds to the onset of the reversal of the exchange anisotropy. The higher transition temperature, $T_{B,c} \sim 180$ K, is the blocking temperature of grain cores in the AFM layer. Between both temperatures, the sign of the uncompensated AFM moment is opposite to that induced during the field cooling process.

5. Conclusions

We have observed and measured a positive exchange bias in nanocrystalline Py/Co–O and Py/Ni–O bilayers at temperatures approaching the AFM transition. This effect also appears after magnetic training of the samples at a determined temperature. This phenomenon is qualitatively attributed to the existence of two different transition temperatures in the AFM grains, associated with boundaries and cores, and to the change of sign of the uncompensated moment of the AFM grains after the magnetic transition of boundaries. The observed effect becomes sizeable due to the nanocrystalline nature of the oxide layers. The thermal evolution of hysteresis loop shift and coercivity provides an immediate way of determining and discriminating both the grain boundary and grain core transition temperatures in these nanocrystalline materials.

Acknowledgment

This work has been supported by the Spanish CICyT agency under project MAT98-0965-C04.

References

[1] Meiklejohn W H and Bean C P 1956 *Phys. Rev.* **102** 1413
[2] Nogués J and Schuller I K 1999 *J. Magn. Magn. Mater.* **192** 203
[3] Berkowitz A E and Takano K 1999 *J. Magn. Mater.* **200** 552
[4] Dieny B *et al* 1991 *J. Appl. Phys.* **69** 4774
[5] Nogués J, Lederman D, Moran T J and Schuller I K 1996 *Phys. Rev. Lett.* **76** 4624
[6] Kiwi M, Mejia-Lopez J and Portugal R D 2000 *Solid State Commun.* **116** 315–19
[7] Schlenker C and Paccard D 1967 *J. Physique* **28** 611
[8] Nikitenko V I *et al* 1998 *Phys. Rev.* B **57** R8111
[9] Gökemeijer N J, Cai J W and Chien C L 1999 *Phys. Rev.* B **60** 3033
[10] Kiwi M 1999 *J. Magn. Magn. Mater.* **234** 552
[11] Stamps R L 2000 *J. Phys. D: Appl. Phys.* **33** R247–68
[12] Mauri D *et al* 1987 *J. Appl. Phys.* **62** 3047
[13] Stiles M D and McMichael R D 1999 *Phys. Rev.* B **55** 3722
[14] Malozemoff A P 1987 *Phys. Rev.* B **35** 3679
Malozemoff A P 1998 *J. Appl. Phys.* **63** 3874
[15] Takano K *et al* 1997 *Phys. Rev. Lett.* **79** 1130
[16] Liu K *et al* 2001 *Phys. Rev.* B **63** 060403
[17] Gruyters M and Riegel D 2001 *Phys. Rev.* B **63** 052401
[18] Nogués J, Lederman D, Moran T J and Schuller I K 1996 *Phys. Rev. Lett.* **76** 4624
[19] Navarro E, Hernando A, Yavari A R, Fiorani D and Rosenberg M 1999 *J. Appl. Phys.* **86** 2166
[20] del Bianco L, Ballesteros C, Rojo J M and Hernando A 1998 *Phys. Rev. Lett.* **82** 4500
[21] Lederman D, Ramos C A, Jaccarino V and Cardy J L 1993 *Phys. Rev.* B **48** 8365
[22] Kittel C 1993 *Introduction to Solid State Physics* ed Reverte p 28
[23] Li Z and Zhang S 2000 *Phys. Rev.* B **61** R14897